고체형 꼬리 지느러미로 오스트라키폼 유영을 하는 물고기 로봇의 패러미터 식별 및 성능 분석

Experimental Parameter Identification and Performance Analysis of a Fish Robot with Ostraciiform Swimming Mode using Rigid Caudal Fins

Wai Leung Chan[1], 이 기 건[2], 김 병 하[2], 최 정 민[1], 강 태 삼[†]

Wai Leung Chan[1], Gigun Lee[2], Byungha Kim[2], Jung Min Choi[1], Taesam Kang[†]

Abstract The ostraciiform swimming mode allows the simplest mechanical design and control for underwater vehicle swimming. Propulsion is achieved via the flapping of caudal fin without the body undulatory motion. In this research, the propulsion of underwater vehicles by ostraciiform swimming mode is explored experimentally using an ostraciiform fish robot and some rigid caudal fins. The effects of caudal fin flapping frequency and amplitude on the cruising performance are studied in particular. A theoretical model of propulsion using rigid caudal fin is proposed and identified with the experimental data. An experimental method to obtain the drag coefficient and the added mass of the fish robot is also proposed.

Keywords : Underwater Vehicles, Ostraciiform, Rigid Caudal Fin, Added Mass, Drag Coefficient

1. Introduction

In the underwater vehicle technology[1], efficient and low noise propulsion features are highly desired for marine exploration and surveillance. After around 400 million years of evolution[2], it is no doubt that fishes have developed the superior biological mechanism to move effectively and quietly in the aquatic environments. The propulsive efficiencies for dolphins and phocid seals swimming in the thunniform mode range from 0.77 to 0.92[24-27], while those of conventional propellers are from 0.4 to 0.5[23]. Therefore, fish swimming[3] is a candidate that can be incorporated into underwater vehicles design to improve the motion performance in water.

Received : Apr. 26. 2010; Reviewed : May. 25. 2010; Accepted : Jun. 11. 2010
※ This work was supported by the Korea Research Foundation Grant (KRF-2006-005-J03303).

† Corresponding Author : Department of Aerospace Information Engineering, Konkuk University.(Email : tskang@konkuk.ac.kr)
[1] Artificial Muscle Research Center, Konkuk University.
[2] Department Of Aerospace Information Engineering, Konkuk University.

Typical fish locomotion for cruising usually belongs to BCF propulsion type[4, 5, 6], which relies on the body undulatory and caudal fin flapping motions. Depending on the body participation in the undulatory motion, several swimming modes can be classified within the BCF. Anguilliform (e.g. eel) moves its whole body to form a wave shape (snake-like) for thrust. Carangiform (e.g. salmon) and thunniform (e.g. shark) confine the undulatory motion on their rear half-body and tail parts for high-speed swimming. Ostraciiform (e.g. boxfish) purely attains the propulsion by caudal fin oscillation. Modelling of fish motion can be found in[15-17], mechanics and control review in[18], applications of composite materials in[19-21], and direction control of a fish robot using robust control scheme in[22].

Within BCF, the ostraciiform swimming mode allows the simplest mechanical design for fish mimicking underwater vehicles. Both cruising and turning motion can be achieved via the caudal fin oscillation. Such swimming

mode can be implemented to an existing underwater vehicle design by attaching an artificial fin to its rear with suitable flapping mechanism.

Thrust is one of the important measures for the effectiveness of caudal fin propulsion. During flapping, water around the caudal fin is accelerated; and forms the Karman Vortex Street [7], which in turn propels the underwater vehicle. When the vehicle is moving at its terminal velocity, the average thrust is balanced by the hydrodynamic drag. Hence, the swimming thrust can be determined indirectly from the terminal velocity.

Several factors can influence the thrust strength of a swimming underwater vehicle. From the vehicle body aspect, the hydrodynamic drag will reduce the vehicle speed due to energy lost and the added mass leads to lower acceleration. In caudal fin aspect, the geometry and material can highly affect the formation of Karman Vortex Street for thrust generation. With a given design of vehicle and fin, the tuning parameters for the swimming motion will be the flapping frequency and amplitude.

In this research, the thrust generation of underwater vehicles using ostraciiform locomotion was explored experimentally. An ostraciiform fish robot and four different caudal fins were applied to investigate the effects of flapping frequency and amplitude on the cruising performance. The swimming motion was restricted to 2D to eliminate other influences on the propulsion. The added mass and drag coefficient of the fish robot were also determined through an experimental setup. A mathematical model of caudal fin propulsion was derived to compare with experimental results. Since caudal fins can suffer various degree of bending for different materials and thickness, the modeling of fin oscillation in water is tedious in general. To simplify the modeling and experimental comparisons, all caudal fins are rigid in both the experiments and modeling.

Nomenclature

A Frontal cross-sectional area of fish robot (cm^2)
A_w Peak to peak wake amplitude (= $2L\ sin\theta_{max}$) (cm)
C_d Drag coefficient of fish robot
E_{wacc} Energy delivered for water acceleration (W)
f Flapping frequency (Hz)
f_c Friction of the fixed pulleys system (N)
F_p Swimming propulsive force (N)
g Earth's gravity = 980cm/s
H Height of caudal fin (cm)
I_h Hydrodynamic moment of inertia of caudal fin(g cm^2)
L Length of caudal fin (cm)
L_0 Gap between axle and caudal fin (cm)
m_a Added mass of fish robot (g)
m_f Inertia mass of fish robot (g)
m_p Inertia contribution from the fixed pulleys system (g)
m_w Mass of pulling weight (g)
P_{ave} Average power for propulsion (W)
R_v Ratio of average velocity to terminal velocity = v_a / v_∞
v_a Average velocity (cm/s)
v_∞ Terminal velocity (cm/s)
η Energy efficiency in the water recoil process
θ Flapping angle
θ_{eff} Effective flapping amplitude = $\theta_{max} - \theta_{off}$
θ_{max} Flapping amplitude (maximum flapping angle)
θ_{off} Flapping amplitude offset
ρ_w Density of water = 0.997g/cm^3

2. Model of Propulsion with Rigid Caudal Fin

The ostraciiform swimming mode is characterized by the oscillation of caudal fin for swimming propulsion. This mode can be implemented to an underwater vehicle by attaching a caudal fin to the rear with suitable flapping mechanism. As shown in Fig. 1, the caudal fin angle $\theta(t)$ is defined to be the angular displacement of the fin measured from the longitudinal axis of the underwater vehicle. The simplest description for flapping is harmonic oscillation and the motion can be described by

$$\theta(t) = \theta_{max} \sin(2\pi f t) \tag{1}$$

The oscillation will accelerate the water around the fin. For an infinitesimal angular displacement $d\theta$, the energy delivered for the water acceleration is

$$dE_{wacc} = -I_h \ddot{\theta} d\theta = 4\pi^2 f^2 I_h \theta\, d\theta\,. \tag{2}$$

The accelerated water forms Karman Vortex Street,

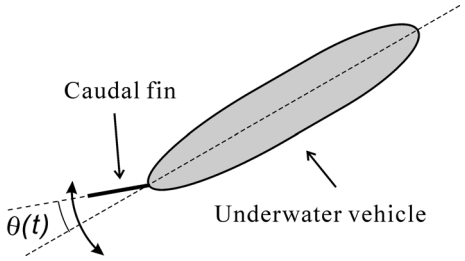

Fig. 1. The flapping angle

which transfers some kinetic energy back to the underwater vehicle for thrusting. Hence, the propulsion can be treated as the recoil from the accelerated water. Assuming that the efficiency of the recoil process is independent of the flapping frequency and amplitude, the average power delivered for swimming propulsion is

$$P_{\text{ave}} = (4\eta / T)\int_0^{\theta_{\max}} dE_{wacc} = 8\eta\pi^2 f^3 I_h \theta_{\max}^2 . \quad (3)$$

When the vehicle reaches its terminal velocity, the kinetic energy is dissipated to the hydrodynamic drag. Therefore,

$$8\eta\pi^2 f^3 I_h \theta_{\max}^2 = 0.5\rho_w C_d A v_\infty^3 , \quad (4)$$

and thus

$$v_\infty^3 = \frac{16\eta\pi^2 I_h}{\rho_w C_d A}\theta_{\max}^2 f^3 . \quad (5)$$

From (5), the intrinsic factors that affect the terminal velocity are related to the geometry of the vehicle (C_d and A) and caudal fin (I_h), which have definite values for a given design of underwater vehicle; the external factors that one can change the terminal velocity are the flapping frequency f, and the flapping amplitude $\theta_{\max}$.

The hydrodynamic moment of inertia of a caudal fin with arbitrary shape is generally obtained from computational fluid dynamics[8]. Depending on the material and thickness, the fin may suffer different degree of bending and this gives an extra complexity in the computational process. To simplify the modeling of propulsion, it is assumed that the caudal fin is rigid. In this case, the analytical expressions of hydrodynamic moment of inertia for some simple geometries can be found in[9]. For a rectangular laminar plate, the hydrodynamic moment of inertia is given by

$$I_h = (9/128)\rho_w \pi\left[\left(L + L_0\right)^4 - L_0^4\right]H . \quad (6)$$

In this research, the effects of flapping frequency and amplitude were explored to validate the propulsion model in (5). Some rigid rectangular caudal fins were used to determine the water recoil efficiency η.

3. Experiments and Setup

The experiments were carried out in a circular inflatable pool with the diameter of 154cm and depth of 25cm. An ostraciiform fish robot was employed for the underwater vehicle. Propulsion was initiated upon the reception of wireless command signals from a host computer.

3.1 Underwater Vehicle Design

The underwater vehicle used for the experiments was an ostraciiform fish robot as shown in Fig. 2. The robot is a boxfish type with rigid acrylic frame. The body section and rear section have constant thickness from the side view and are symmetric from the front and top views.

Inside the body of the robot are electronic components for motion control and data acquisition. The rear section has an electro-mechanical system, which consists of a waterproofed servo, axle and some mechanical linkages, for generating caudal fin oscillation. Two clips are mounted on the axle for caudal fin replacements.

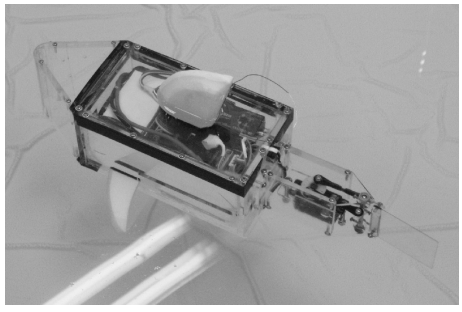

Fig. 2. The ostraciiform fish robot

Additional weight was placed inside the body for orientation balance and buoyancy adjustment. The dorsal fin prevented the robot from sinking and maintained the top surface of the robot body about 3cm below the water surface. Therefore, the robot was performing 2D swimming motion. Pectoral fins were attached to increase damping in the rolling and vertical motions. Table 1 summarizes the mechanical properties of the ostraciiform fish robot.

TABLE 1. Mechanical Properties of the ostraciiform Fish Robot

Description	Property
Body material	Acrylic
Caudal fin material	Acrylic
Pectoral and dorsal fins material	PVC foam
Total length (caudal fin excluded)	26.4cm
Width of fish robot body (pectoral fins excluded)	7.4cm
Height of fish robot body (dorsal fin excluded)	8.8cm
Caudal fin thickness	1mm
Distance between caudal fin clips	4cm
Gap between axle and caudal fin L_0	0.7cm
Inertial mass m_f	1196g
Frontal cross-sectional area in water A	69.8cm^2

3.2 Caudal Fins

To identify the propulsion model in (5), four 1mm thick acrylic caudal fins were applied for the swimming study. Three fins (2025Rect, 2925Rect and 3825Rect) are rectangular with different size while the last one (2925Arb) has an arbitrary profile on one side as shown in Fig. 3. The caudal fin 2925Arb is used to confirm the validity of (5) further. The aspect ratios (height^2/area) of all fins are 2 and Table 2 summarizes their dimension. All fins can be treated as rigid with the choice of material, thickness, and size in the experiments.

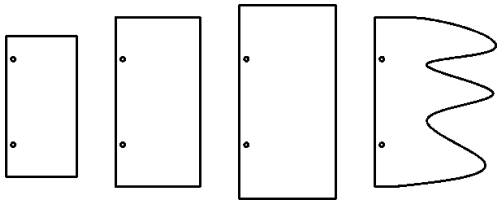

Fig. 3. Caudal fin: 2025Rect, 2925Rect, 3825Rect, and 2925Arb(from left to right)

TABLE 2. Dimension and aspect ratio (AR) of caudal fins

Name	Height H (cm)	Length L (cm)	Area (mm^2)	AR
2025Rect	6.36	3.18	2025	2
2925Rect	7.65	3.82	2925	2
3825Rect	8.75	4.37	3825	2
2925Arb	7.65	5.64	2925	2

3.3 Set up for Added Mass and Drag Coefficient Determination

Fig. 4 shows an experimental setup to measure the added mass and drag coefficient of the fish robot. The robot was connected to a pulling weight (mass = m_w) with a string routed through a fixed pulleys system. Seven different pulling weights (10g to 40g in a step of 5g) were used in the displacement measurements. The fish robot and the pulling weight were holding static until the displacement measurement started ($x(0) = v(0) = 0$). When the weight fell, it generated a constant pulling force on the robot and caused the robot to cruise straight toward the bottom pulley. An optical encoder circuit recorded the motion of a pulley with time. The displacement (with the resolution of 0.785cm) of the robot and pulling weight can be obtained accordingly. The zero position is set just after the signal click output of the optical encoder in order to minimize the uncertainty between the first measurement point and zero position point. By comparing the measurement data with a theoretical model as derived in the later section, the added mass and drag coefficient can be determined.

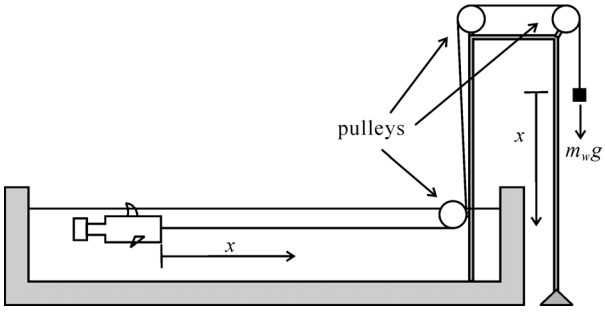

Fig. 4. Experimental setup for added mass and drag coefficient determination

3.4 Average Velocity Measurements

Due to the limited pool size, it is not possible for the fish robot to swim at its terminal velocity. Nevertheless, as it will be shown later, the terminal velocity can be determined indirectly from the average velocity.

As shown in Fig. 5, in each average velocity measurement, the fish robot swam forward for 115cm (x_f = 115cm) from rest ($x(0) = v(0) = 0$) and the swimming motion was recorded in video for time measurement (with the error of ±0.1s). In general, the average velocity can be determined in the section of $x_f - x_i$, where x_i is choosen between $x(0)$ and x_f . To minimize the measurement error, the position of x_i was chosen the same as the starting position (i.e. $x_i = x(0)$ = 0cm). The measurement was focused on the velocity along the x direction. As the fish robot navigate along the x direction, there was also motion along the y direction. This problem was solved by slightly adjusting the dorsal fin.

To compare the experimental results with the model (5), the average velocity of the fish robot was measured for different frequency and amplitude settings. One flapping parameter (frequency or amplitude) was fixed to study the effects of the other. For the fixed amplitude of 16 degree, the frequency was set from 1.5Hz to 4.0Hz in a step of 0.5Hz. Therefore, there were six measurements for each caudal fin. To study the effects of flapping amplitude on the average velocity, two frequencies (2.5Hz and 3.5Hz) were selected for different flapping amplitudes.

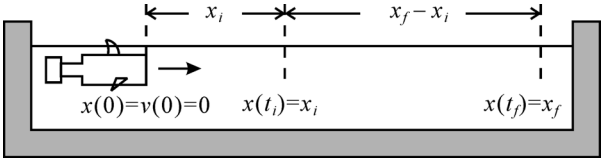

Fig. 5. Experimental setup for average velocity measurements

4. Results and Analysis

4.1 Added Mass and Drag Coefficient Determination

The experimental data (down-sampled discrete points) for the added mass and drag coefficient determination are plotted in Fig. 6 for different pulling weights.

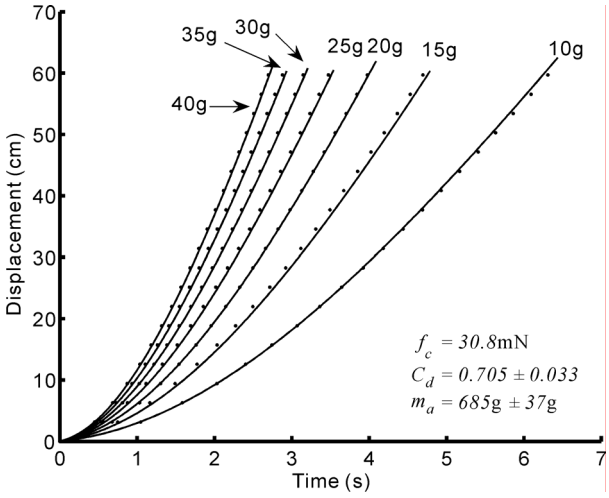

Fig. 6. Experimental results (discrete points) and the theoretical simulated outputs using the identified coefficients and same pulling weight inputs(bold)

From the experimental setup as shown in Fig. 4, it is assumed that the air drag on the pulling weight is negligible, the equation of motion can be written as[14]:

$$M\ddot{x} + 0.5\rho_w C_d A\dot{x}^2 = m_w g - f_c, \tag{7}$$

$$M = m_f + m_a + m_w + m_p, \tag{8}$$

where the inertia contribution from the fixed pulley system m_p is 20g. With the initial conditions ($x(0) = v(0) = 0$), the solution for the displacement and velocity are:

$$x(t) = a_1^{-1} \ln\left[\cosh\left(\sqrt{a_1 a_2}\, t\right)\right], \tag{9}$$

$$v(t) = \dot{x}(t) = \sqrt{a_2 / a_1}\, \tanh\left(\sqrt{a_1 a_2}\, t\right), \tag{10}$$

$$a_1 = \rho_w C_d A / (2M), \tag{11}$$

$$a_2 = (m_w g - f_c) / M\ . \tag{12}$$

The velocity in (10) can be rewritten in term of the displacement as

$$v^2(m_w,x) = (a_2/a_1)\tanh^2\left[\varphi(x)\right] = \alpha(x)m_w - \beta(x) \quad (13)$$

where

$$\varphi(x) = \sqrt{a_1 a_2}\,t = \cosh^{-1}\left[\exp(a_1 x)\right]. \quad (14)$$

$$\alpha(x) = \left[2g/(\rho_w C_d A)\right]\tanh^2\left[\varphi(x)\right], \quad (15)$$

$$\beta(x) = \left[2f_c/(\rho_w C_d A)\right]\tanh^2\left[\varphi(x)\right]. \quad (16)$$

In the experiments, since the mass of pulling weight ($m_w \le 40$g) is much smaller compared to the vehicle weight (m_f = 1196g), the parameters M and a_1 in (8) and (11) can be treated as constants with respect to the weight. Accordingly, the values of $\varphi(x)$, $\alpha(x)$ and $\beta(x)$ are nearly independent of m_w, and (13) becomes a linear equation of m_w. From (15) and (16), the friction of the fixed pulleys system can be determined by

$$f_c = g\beta(x)/\alpha(x). \quad (17)$$

At a given pulling weight, if two displacement points ($x_1 = x(t_1)$ and $x_2 = x(t_2)$) are chosen, the following equation can be obtained from (13) and (14)

$$\frac{v^2(m_w,x_1)}{v^2(m_w,x_2)} = \frac{1-\exp(-2a_1x_1)}{1-\exp(-2a_1x_2)}. \quad (18)$$

If $x_2 = 2x_1$, the analytical expression of a_1 can be expressed as

$$a_1 = -(2x_1)^{-1}\ln\left(v^2(m_w,x_2)/v^2(m_w,x_1) - 1\right). \quad (19)$$

In general, the value of a_1 can be obtained by solving (18) using Newton's method. Once the value of a_1 is available, the value of a_2, added mass m_a and drag coefficient C_d can be determined from (8) and (11) – (14) thereby.

From the experimental data as shown in Fig. 6, two different displacement points, x_1 = 29.3cm and x_2 = 58.4cm, were chosen for each pulling weight. The velocity was determined using linear curve fitting with the data around these two displacement points. Fig. 7 shows the velocity square versus the mass of pulling weight (discrete points) and the best-fit lines. The pulley friction, which can be determined from the slope and y-intercept of the two best-fit lines according to (13) and (17), is 30.8mN on average. Hence, the values of the drag coefficient and added mass are 0.705±0.033 and 685±37g respectively. The added mass depends on geometry of the body. Formulas for typical shape can be found in [9]. Assuming rectangular type, the rough estimate of the added mass of the fish robot is 764 g. The known drag coefficient of a cube is 0.8[13]. Both the measured added mass and drag coefficient of the fish robot are both similar to the theoretical estimates and thus the values obtained are reasonable.

With the experimental determined values of f_c = 30.8mN, C_d = 0.705 and m_a = 685g, the theoretically estimated curves (bold) as computed by (7) and (9) are plotted in Fig. 6 for each pulling weight. It can be seen that the model (7) with the identified coefficients and with solution (9) fits well with the experimental results.

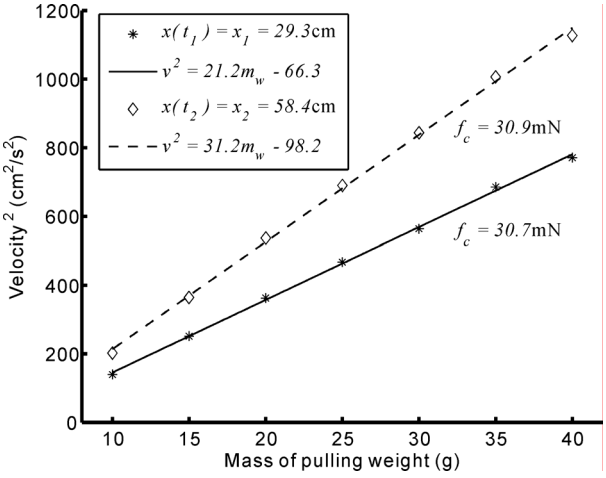

Fig. 7. Velocity square versus mass of pulling weight (discrete points) and best-fit lines

4.2 Average Velocity Measurements

As shown in Fig. 5, the equation of motion and the solution for the underwater water vehicle swimming forward with the initial conditions ($x(0) = v(0) = 0$) are

$$(m_f + m_a)\ddot{x} + 0.5\rho_w C_d A\dot{x}^2 = F_p \quad (20)$$

$$x(t) = b_1^{-1} \ln\left[\cosh\left(\sqrt{b_1 b_2}\, t\right)\right], \quad (21)$$

$$v(t) = \dot{x}(t) = \sqrt{b_2 / b_1}\, \tanh\left(\sqrt{b_1 b_2}\, t\right) = v_\infty \tanh\left(\sqrt{b_1 b_2}\, t\right), \quad (22)$$

$$b_1 = 0.5\rho_w C_d A / (m_f + m_a), \quad (23)$$

$$b_2 = F_p / (m_f + m_a). \quad (24)$$

For the average velocity measured between two different displacement points (x_i and x_f), it can be shown from (21) that the average velocity is proportional to the terminal velocity as

$$v_a = R_v(x_i, x_f) v_\infty = \frac{b_1(x_f - x_i)}{\cosh^{-1}(\exp(b_1 x_f)) - \cosh^{-1}(\exp(b_1 x_i))} v_\infty. \quad (25)$$

Note that the influences of caudal fin geometry and flapping parameters are reflected in the propulsion force F_p, which in turn affects the terminal velocity v_∞, but not the velocity ratio $R_v(x_i, x_f)$ for a given set of x_i and x_f. Incorporating (25) into (5) gives

$$v_a^3 = [R_v(x_i, x_f) v_\infty]^3 = \frac{16\eta\pi^2 I_h}{\rho_w C_d A} \theta_{\max}^2 f^3 R_v^3(x_i, x_f). \quad (26)$$

For b_1 = 0.0130cm^{-1} as computed by (23), x_i = 0cm and x_f = 115cm, the average velocity is 68.8% of the terminal velocity, i.e. R_v = 0.688, and the maximum percentage error of the average velocity is 1.05% with the measurement errors δx_i = 0cm and δx_f = ±4cm. Hence, the value of R_v is relatively not sensitive to the displacement error of ±4cm and R_v = 0.688 was applied throughout the analysis in this research.

Fig. 8 shows the average velocity versus the flapping frequency and the best-fit lines (with the constraint of zero y-intercept) for constant flapping amplitude of 16 degree. The experimental results show that the average velocity (and hence the terminal velocity) is proportional to the frequency, which is consistent with the description in (26). Larger caudal fin, in general, yields higher average velocity due to larger hydrodynamic moment of inertia. The 2925Arb is slower the 2925Rect even for the same aspect ratio and area. The highest average velocity (= 9.67cm/s) is obtained by using the 3825Rect flapping at 4Hz, which gives the terminal velocity of 9.67/0.688 = 14.06cm/s. Note that the average velocities at 4 Hz are all smaller than curve-fitted values due to the non-rigid characteristics of the caudal fins at high frequency.

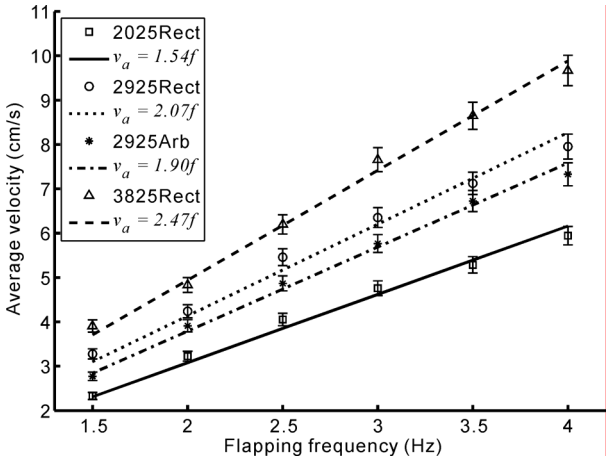

Fig. 8. Experiment measurements of average velocity (discrete points) versus the flapping frequency with the best-fit lines for $\theta_{\max}$ = 16°

4.3 Effects of Flapping Amplitude on Average Velocity

Fig. 9 and 10 show that the experimental data and the best-fit lines of the average velocity to the power of 1.5 ($v_a^{1.5}$) versus the flapping amplitude for the frequency of 2.5Hz and 3.5Hz respectively. In both cases, there exists a linear relationship between the $v_a^{1.5}$ and flapping amplitude. Each best-fit line shows a finite value of x-intercept, which indicates the existence of amplitude offset θ_{off} in the flapping motion. Table 3 summarizes the

TABLE 3. Flapping Amplitude offset (deg) for propulsion

Caudal fin name	2.5Hz	3.5Hz
2025Rect	5.43	5.49
2925Rect	5.27	5.10
2925Arb	5.71	5.71
3825Rect	5.47	5.19

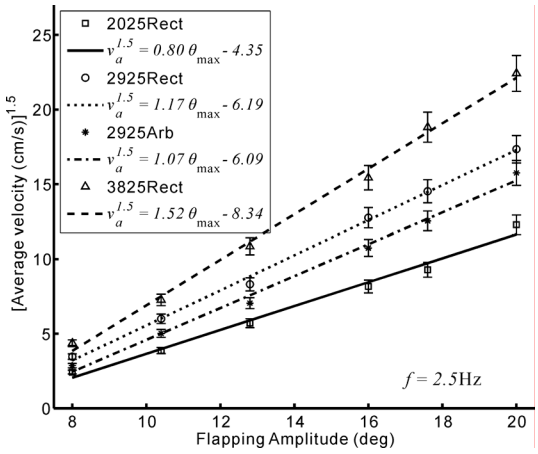

Fig. 9. Experiment measurements of [average velocity]$^{1.5}$ (discrete points) versus θ_{max} with the best-fit lines for f = 2.5Hz

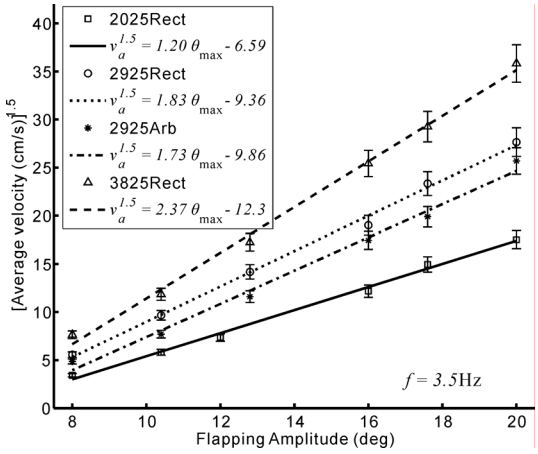

Fig. 10. Experiment measurements of [average velocity]$^{1.5}$ (discrete points) versus θ_{max} with the best-fit lines for f = 3.5Hz

amplitude offset determined from Fig. 9 and 10; the offset is found around 5.42°±0.22° for all caudal fins and frequencies.

4.4 Efficiency of Water Recoil Process

Due to the existence of amplitude offset, (26) is modified to

$$v_a^3 = \frac{16\eta\pi^2 I_h}{\rho_w C_d A}\left(\theta_{\max} - \theta_{\text{off}}\right)^2 f^3 R_v^3(x_1, x_2), \\ = \frac{16\eta\pi^2 I_h}{\rho_w C_d A}\theta_{\text{eff}}{}^2 f^3 R_v^3(x_1, x_2). \tag{27}$$

With the parameters (C_d = 0.705, θ_{off} = 5.42° and R_v = 0.688) determined previously, the energy efficiency of water recoil process, i.e., the ratio of the energy used for the propulsion versus the energy delivered to the caudal fin, for the three rectangular fins in Fig. 8 to 10 can be computed using (6) and (27) and are listed in Table IV. Note that the energy consumed by the driving motor is not included. Efficiencies with 2 Hz driving are obtained using data in Fig. 8. The average efficiency is around 34.1 %. Fig. 9 shows a slightly higher values compared to the other two figures. This may suggest the fish robot can swim more effectively at frequency of 2.5 Hz.

TABLE 4. Efficiency of Water Recoil Process with θ_{max} = 16° (%)

Data Source / Fin	Fig. 8 (2 Hz)	Fig. 9 (2.5 Hz)	Fig. 10 (3.5 Hz)
2025Rect	31.0	38.8	31.9
2925Rect	34.0	38.0	33.8
3825Rect	32.2	35.4	31.3

4.5 Propulsive Force

The propulsive force is balanced by the hydrodynamic drag when the vehicle is travelling at its terminal velocity, which can be determined from the average velocity indirectly though (25) with R_v = 0.688 in the experiments. Fig. 11 shows the propulsive force of the ostraciiform fish robot corresponding to Fig. 8. The force is ranged from 2.81mN to 48.42mN and increased with the frequency quadratically. The 2025Rect yields the weakest thrust

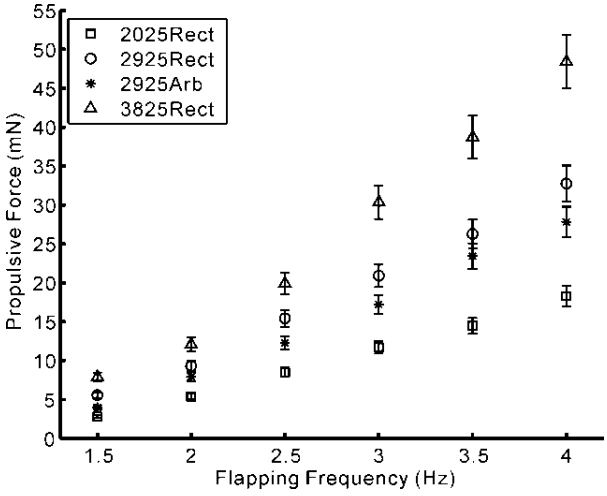

Fig. 11. Propulsive force versus flapping frequency for θ_{max} = 16°

while the 3825Rect is the strongest fin for cruising among the four fins.

4.5 Strouhal Number

The Strouhal number is a dimensionless parameter defined as

$$S_t = fA_w / v_t . \quad (28)$$

It measures the effectiveness of swimming motion and the optimal value is within the range of 0.25 to 0.4[10]. Note that the velocity used in (28) is the terminal velocity instead of average velocity, which is significantly (31.2%) lower than the terminal velocity in the experiments. The Strouhal number versus the flapping frequency corresponding to Fig. 8 is plotted in Fig. 12. For each fin, the number is quite constant to the frequency due to the proportionality of terminal velocity to flapping frequency as shown in Fig. 8. Among the four caudal fins, the 3825Rect is near to the desired one as long as Strouhal numbers are concerned. All rectangular caudal fins yield the Strouhal number, from 0.74 to 1.00, which is far from the optimal range. For the 2925Arb, the values of S_t are exceptionally high due to the large value of fin length (see Table 2) in A_w computation. The effective wake amplitude and hence the Strouhal number should be smaller for such an extreme fluctuated fin profile.

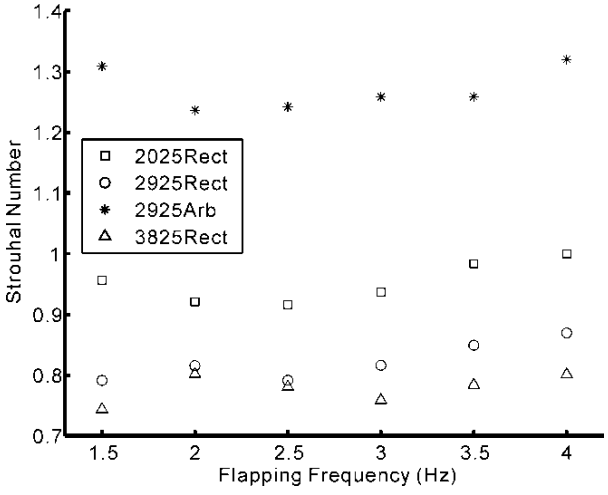

Fig. 12. Strouhal number versus flapping frequency for θ_{max} = 16°

5. Discussion

5.1 Drag coefficient

The experimental setup in Fig. 4 is a simple method to determine both the drag coefficient and added mass of small- scale underwater vehicles without using force sensors or load cells. The drag coefficient of the fish robot (0.705) is quite high compared to natural species [11, 12] due to the inefficient hydrodynamic body shape. The similar experimental work can be setup in indoor swimming pool for medium scale underwater vehicle (~1m long).

5.2 Energy Efficiency of Water Recoil Process

The energy efficiency of the water recoil process obtained in section IV-B is independent of the type of actuators as long as the actuation can provide the required flapping frequency and amplitude. It depends on the geometry and material of the fin and is an evaluation of caudal fins performance in the process of energy transfer from accelerated water (which forms Karman Vortex Street) to the kinetic energy of the fish robot.

5.3 Flapping Amplitude Offset

The nonzero y-intercepts in Fig. 9 and 10 indicate that there exists an offset (about 5.42 degree) in flapping amplitude for propulsion in the experiments. The first reason is due to the backlash, which is accounting for about 2 degree. The second reason is the inability of Karman Vortex Street generation due to small wake amplitude. The last reason is the oscillation of fish robot body during the swimming motion. As shown in Fig. 13, the vehicle body gains some angular momentum from the oscillating fin and hence, will oscillate during the ostraciiform swimming. Such oscillation will reduce the effective wake amplitude for vortices generation.

From Table 3, there is no observable dependence of amplitude offsets on the flapping frequency and amplitude. The dependence may exist but not revealed significantly in the experiment data. Note that the

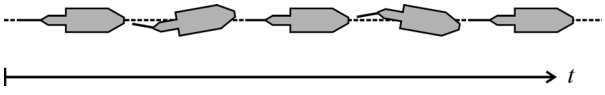

Fig. 13. Oscilation of fish robot body in ostraciiform swimming mode

undulatory motion of the tail fin inevitably invokes the oscillatory motion vertical to the swimming direction, and this should be considered for more detailed investigation.

5.4 Effectiveness of Swimming Motion

The ostraciiform mode is not, biologically, the most efficient swimming mode in the BFC propulsion. From Fig. 12, the high values of Strouhal number reflect the ineffective swimming motions performed by the fish robot in the experiment. Beside the biological reason, the inefficient hydrodynamic profile of the fish robot body and the unfavorable generation of Karman Vortex Street by rigid caudal fins could contribute to the poor performance.

The underwater vehicle body oscillation is unavoidable in ostraciiform mode due to the nature of propulsion mechanism. The oscillation could be damped with heavier and larger hydrodynamic moment of inertia of underwater vehicle body compared to caudal fin, however, the maneuvering ability and acceleration will be diminished accordingly. Optimal design of body shape for ostraciiform has to balance all these adverse effects.

6. Conclusions

The propulsion of ostraciiform swimming mode underwater vehicles with rigid caudal fin is studied through the average velocity measurements. An ostraciiform fish robot, with added mass of 685±37g and drag coefficient of 0.705±0.033, is employed for the underwater vehicle. Four different rigid caudal fins are applied in the average velocity measurements. Minimum flapping amplitude (amplitude offsets) exists due to inability of Karman Vortex Street generation, mechanical backlash and body oscillatory motion during swimming. Experimental data shows that the average velocity is proportional to the flapping frequency for constant flapping amplitude. For a given flapping frequency, the average velocity to the power of 1.5 is proportional to the effective flapping amplitude. The results are well agreed with a mathematical model of rigid caudal fin propulsion. The research in this paper is restricted to the one dimension motion only and further research to describe the two dimensional motion is to be conducted for more accurate motion modeling of the fish robot.

참고문헌

[1] R. Bandyopadhyay, “Trends in Biorobotic Autonomous Undersea Vehicles”, IEEE Journal of Oceanic Engineering, Vol.29, pp.1-32, 2004.

[2] B.G.M. Jamieson, Fish Evolution and Systematics: Evidence from Spermatozoa, Cambridge University Press, Cambridge, 1991.

[3] M. Sfakiotakis, D. M. Lane and J. C. Davies, “Review of Fish Swimming Modes for Aquatic Locomotion”, IEEE Journal of Oceanic Engineering, Vol.24, No.2, pp.237-252, 1999.

[4] P.W. Webb, “Swimming”, in The Physiology of Fishes 2nd Edition, D.H. Evans Ed., pp.3-24, CRC Press, Boca Raton, Florida, 1998.

[5] P.W. Webb, “The Biology of Fish Swimming”, in Mechanics and Physiology of Animal Swimming, L. Maddock, Q. Bone, and J. M. V. Rayner Eds, pp.45-62, Cambridge University Press, Cambridge, UK.

[6] G.S. Helfman, B.B. Collette and D.E. Facey, “The Diversity of Fishes”. Blackwell Science, Inc., Malden, Massachusetts, 1997.

[7] R.W. Blake, Fish Locomotion, Cambridge University Press, 1983.

[8] J.H. Ferziger and M. Peric, Computational methods for fluid dynamics, Springer, 1999.

[9] C. E. Brennen, “A Review of Added Mass and Fluid Inertial Forces”, Naval Civil Engineering Laboratory, CR82.010, January 1982.

[10] G. S. Triantafyllou, M. S. Triantafyllou and M. A. Grosenbauch, “Optimal thrust development in oscillating foils with application to fish propulsion”, Journal of Fluids Structure., Vol.7, pp.205-224, 1993.

[11] J.Gray, “Studies in Animal Locomotion VI. The Propulsive Powers of the Dolphin”, Journal Expl. Biol., Vol.13, pp.192-199, 1936.

[12] D. Bilo and W. Nachtigall, “A Simple Method to Determine Drag Coefficients in Aquatic Animals”, J. Exp, Biol. Vol.87, pp.357-359, 1980.

[13] http://www.engineeringtoolbox.com/drag-coefficient-d_627.html.

[14] T. J. Pedley, and S. J. Hill, “Large–amplitude undulatory fish swimming: fluid mechanics coupled

to internal mechanics", The Journal of Experimental Biology, Vol.202, pp.3431−3438, 1999.

[15] Junzhi Yu, Shuo Wang and Min Tan, "A simplified propulsive model of bio-mimetic robot fish and its realization," Cambridge University Press, Robotica, Vol.23, pp.101-107, 2005.

[16] R Mason, J Burdick, "Construction and modelling of a carangiform robotic fish," Experimental Robotics VI, Springer, 235-242, 2000.

[17] K.H. Low, "Modelling and parametric study of modular undulating fin rays for fish robots," Mechanism and Machine Theory, Vol.44, pp.615-632, 2009.

[18] J. Edward Colgate, Kevin M. Lynch, "Mechanics and control of swimming: a review", IEEE Journal of Oceanic Engineering, Vol.29, pp.660-673, 2004.

[19] Q. S. Nguyen, S. Heo, H. C. Park, and D. Byun, "Performance evaluation of an improved fish robot actuated by piezoceramic actuators", Smart Materials and Structures, Vol.19, 2010.

[20] B. Kim, D. H. Kim, J. Jung, J. O. Park, "A biomimetic undulatory tadpole robot using ionic polymer-metal composite actuators", Smart Materials and Structures, Vol.14, pp.1579-1585, 2005.

[21] J. W. Paquette, K. J. Kim, "Ionomeric electroactive polymer artificial muscle for naval applications", IEEE Journal of Oceanic Engineering, Vol.29, pp.729-737, 2004.

[22] M. Hur, T. Kang, W. L. Chan, and J. M. Choi, "H_{∞} controller design of an ostraciiform swimming fish robot," Indian Journal of Marine Sciences, Vol.38, pp.302-307, September 2009.

[23] http://www.solarnavigator.net/propellers.htm

[24] F. E. Fish, "Power output and propulsive efficiency of swimming bottlenose dolphins (Tursiops Truncatus)," Journal of Experimental Biology, Vol.185, pp.179-193, 1993.

[25] P. W. WEBB, Hydrodynamics and energetics of fish propulsion, Fisheris Research Board of Canada, Bulletin 190, pp.1−159, 1975.

[26] G. T. Yates, "Hydrodynamics of body and caudal fin propulsion," In Fish Biomechanics (ed. P. W. Webb and D. Weihs), pp.177−213. New York: Praeger, 1983.

[27] F. E. Fish, S. Innes, and K. Ronald, "Kinematics and estimated thrust production of swimming harp and ringed seals," J. exp. Biol. 137, pp.157−173, 1988.

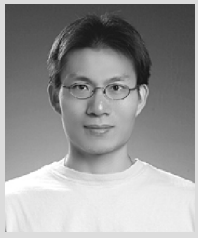

Wai Leung Chan

1997 Physics from the Hong Kong University of Science and Technology (B.S.).

2002, 2005 the University of California, San Diego, USA (M.Sc and Ph.D.).

2006 Researcher&Research Professor, Artificial Muscle Research Center(AMRC), Konkuk University

Research Area : Bio-mimicking robots, swimming study and experiments on autonomous fish robots.

Gigun Lee

2007 Dept. of Mechanical and Aerospace Engineering, Konkuk University (B.S.).

2009 Dept. of Aerospace Information Engineering, Konkuk University (M.S.).

2009~Present Present, Dept. of Aerospace Information Engineering, Konkuk University (Ph.D. student).

Research Area : UAV System, control theory and applications for aerospace, marine, and ground systems.

Byungha Kim

2009 Dept. of Aerospace Information Engineering, Konkuk University (B.S.).

2009~Present Dept. of Aerospace Information Engineering, Konkuk University (Master student).

Research Area : Sensor integration, control system application.

Jung-Min Choi

2005 Chemical Engineering, Kyonggi University (B.S.).

2001 Computer Science, Kyonggi University (M.S.).

2005 Computer Engineering, University of Incheon (Ph.D.).

2006~2007 Research Professor, Chemical Technology Research Center(CTRC), Hankyong National University.

2007~August 2009, Researcher&Research Professor, Artificial Muscle Research Center(AMRC), Konkuk University.

September 2009~Present Researcher, Creative Design Institute(CDI), Sungkyunkwan University.

Research Area : Artificial Intelligent, Electronic Commerce, Data mining, Expert System.

Taesam Kang

1986 Dept. of Control & Instr. Eng., Seoul National University (B.S.).

1988 Dept. of Control & Instr. Eng., Seoul National University (M.S.).

1992 Dept. of Control & Instr. Eng., Seoul National University (Ph.D.).

1994~2001 Associate Professor, Hoseo University.

2001~Present Professor in the Dept. of Aerospace Information Eng., Konkuk University.

Research Area : Sensor design and signal processing, control theory and applications for aerospace, marine, and ground systems.